Dynamics of Foam Films in Constricted Pores

Gurmeet Singh, George J. Hirasaki, and Clarence A. Miller
Dept. of Chemical Engineering, Rice University, Houston, TX 77005

Hydrodynamics of foam films in a porous medium depend strongly on the pore geometry, foam quality, foam flow rate, surfactant formulation, rheological properties of the film, and the capillary pressure in the medium. These dynamics were studied numerically by simulating the behavior of a foam film as it traverses a periodically constricted sinusoidal pore. Different regions of film behavior exist depending on its rheological properties. For a film with rigid (immobile) surfaces, the entrainment effect leads to a thickening film consistent with related phenomena such as Bretherton's (1961) analysis of a bubble moving in a capillary tube. A film with mobile surfaces, however, stretches and thins while remaining uniform in thickness and may become unstable under certain conditions. The dependence of limiting capillary pressure on the foam flow rate and rheological properties is explained quantitatively.

Introduction

Enhanced oil-recovery (EOR) processes seek to extract part of the large amount of unrecovered oil that remains in reservoirs after conventional recovery practices. The efficiency of these processes suffers from channeling, gravity override and viscous fingering of the displacing phase, resulting in poor volumetric sweep of the reservoir. Mobility of a gas flowing through a porous medium is much lower when it is dispersed within a liquid as a foam (Falls et al., 1988; Chambers and Radke, 1992). Consequently foams can improve sweep efficiency in EOR processes. They are also being investigated as a method to improve sweep efficiency of surfactant remediation processes for groundwater aquifers contaminated with organic liquids (Hirasaki et al., 1997).

Falls et al. (1988) define foam in porous media as a "dispersion of gas in liquid such that the liquid phase is interconnected and at least some of the gas flow paths are blocked by lamellae" (i.e., thin liquid films). Foams are classified into two main categories: (1) *continuous*, where there exists at least one flow path for gas that is not blocked by lamellae; and (2) *discontinuous*, where all the flow paths for gas are blocked by lamellae, and thus gas flows as bubbles encapsulated by lamellae (Rossen, 1995; Kovscek and Radke, 1994). In our study we concentrate on *discontinuous* foam composed of individual surfactant-stabilized liquid lamellae, each straddling a pore body or throat and separated from adjacent lamellae by at least a pore length. Curved regions known as plateau borders connect the lamellae to the pore wall. Foam texture in porous media depends on creation and destruction of these lamellae. Foam generation has been discussed in detail by Ransohoff and Radke (1986) and Chambers and Radke (1992). Foam destruction is due to lamella rupture (Chambers and Radke, 1992) and diffusion of gas out of small bubbles. Rossen (1995) emphasizes that foam destruction due to diffusion is insignificant in porous media, "because lamella curvature is not ... related to bubble volume." Experimental observations of Nutt et al. (1992) show that foam flow in porous media is a dynamic process, in which "foam lamellae continually undergo rupture and reconstruction during their passage along the pore system, at rates which are determined by pore geometry, as well as foam quality, foam flow rate and rheological properties of lamellae."

Previous researchers (Khatib et al., 1988) have shown that stability of foam lamellae is limited by capillary pressure in the porous medium. Further, this limiting capillary pressure varies with the surfactant formulation, gas flow rate, and the pore structure of the medium. Jiménez and Radke (1989) presented a hydrodynamic theory to explain the dependence of the limiting capillary pressure on the gas flow rate by analyzing the stability of a foam lamella moving through a periodically constricted sinusoidal pore. They predicted that the foam lamella, as it expands in going from a pore throat to a pore body may thin down to its critical thickness and break. In their model they assumed a foam lamella with plane-parallel surfaces (Ivanov, 1980), and thus were able to use the Reynolds expression (Reynolds, 1886) for the thinning/drainage of the film (lamella).

Correspondence concerning this article should be addressed to G. Singh at the present address: The M. W. Kellogg Co., P.O. Box 4557, Houston, TX 77210.

We present a generalized hydrodynamic model of foam-lamella transport and drainage in a porous medium for the first time. The model accounts for the mobility of the lamella surfaces (Singh, 1996), and reduces to the immobile case (rigid surfaces) under limiting conditions. The numerical model predicts the spatiotemporal evolution of the foam lamella thickness as it traverses a periodically constricted sinusoidal pore for varying parameters—gas flow rate, surfactant formulation, and pore geometry, for example. Results indicate that dynamics of foam lamellae are complex, with contrasting behavior in different regimes of the parameter space. Foam films where the surfactant formulation is such that the films are highly mobile (Singh et al., 1996) show the same dependence of limiting capillary pressure on the gas flow rate as observed by Khatib et al. (1988). In this regime the results are in qualitative agreement with those of Jiménez and Radke (1989). However, the opposite behavior of film thickening due to liquid entrainment is observed for foam lamellae with immobile surfaces. The preceding model can be used to identify surfactant formulations and optimum operating ranges for efficient EOR processes.

This article is organized as follows. We first present the dimensionless equations governing the hydrodynamics of a foam lamella translating in a periodically constricted sinusoidal pore. In the third section we look at the dimensionless parameters affecting foam-film hydrodynamics. This is followed by a note on the numerical technique used to develop the simulator. In the sixth section we present and discuss the results of our simulations under various conditions. In the last section we present the conclusions of this study.

Governing Equations

In this section we present the dimensionless equations governing the hydrodynamics of the foam lamella as it traverses a periodically constricted sinusoidal pore (Figure 1). Lubrication approximation has been invoked in the derivation of these equations, and further for the sake of analysis we assume that the shape of the pore changes gradually. The pore geometry considered is shown in Figure 1 and is quantitatively given as

$$R_p(x) = R_t\left[(1+\beta) - \beta\cos\left(\frac{\pi x}{L}\right)\right], \qquad (1)$$

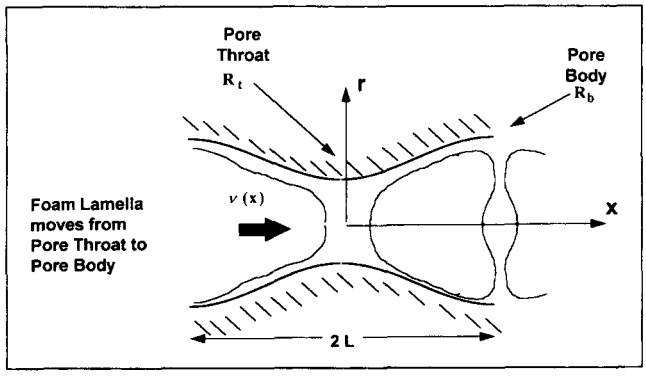

Figure 1. Foam lamella in a periodically constricted sinusoidal pore.

R_t, R_b are the pore throat and body radii, respectively.

where

$$\beta = 0.5\left(\frac{R_b}{R_t} - 1\right),$$

where R_b and R_t are the pore body and pore throat radii, respectively, and L is the axial distance between the pore throat and the pore body; we prefer calling it the pore length. The local interstitial velocity of the foam lamella, $v(x)$, is given as

$$\frac{dx}{dt} = v(x) = \frac{Q}{\pi R_p(x)^2}.$$

Using this relation between the axial location x and time t, we transform the governing equations (Appendix A). From these we obtain the dimensionless governing equations that we use in our numerical model to study the hydrodynamics of the foam lamella. These equations are as follows.

Thickness equation

$$\frac{\partial H}{\partial X} = -\frac{1}{Ca_x}\frac{1}{R}\frac{\partial}{\partial R}(RVH) + \frac{1}{Ca_x}\frac{1}{R}\frac{\partial}{\partial R}\left(RH^3\frac{\partial P}{\partial R}\right) - \frac{1}{R_p}\frac{dR_p}{dX}\left(H - R\left(\frac{\partial H}{\partial R}\right)\right), \qquad (2)$$

where

$$H = \frac{h}{R_p(X)},\ R = \frac{r}{R_p(X)},\ V = \frac{v_r^s}{v_o},\ P = \frac{p - p_g}{P_o(X)},\ X = \frac{x}{L},$$

where h is the film half thickness; v_o is the characteristic surface velocity (Appendix A); $P_o(X) = \sigma/R_p(X)$ is the characteristic pressure, while p and p_g are the pressures in the film (liquid phase) and the gas, respectively. In the analysis p_g is assumed to be constant and Ca_x, the axially dependent capillary number, is given as

$$Ca_x = \frac{3\mu Q}{\pi\sigma L R_p(X)}. \qquad (3)$$

Normal stress balance

$$P = -\frac{1}{R}\frac{\partial}{\partial R}(R\sin\alpha) + \Pi, \qquad (4)$$

where

$$\sin\alpha = \frac{\dfrac{\partial H}{\partial R}}{\left[1 + \left(\dfrac{\partial H}{\partial R}\right)^2\right]^{1/2}}$$

and $\Pi = \Pi(H)$ is the disjoining pressure (Jiménez and Radke, 1989; Joye et al., 1992; Appendix B) and is given as follows:

$$\Pi = \left(\frac{\Pi^o_{el}}{P_o(X)}\right)\left[-\frac{1}{\theta_x H^3} + e^{-\alpha_x H}\right], \qquad (5)$$

where θ_x can be termed the ratio of electrical double-layer forces to van der Waals forces and α_x is a dimensionless inverse Debye length. The parameter Π^o_{el} is defined in Appendix B:

$$\theta_x = \frac{48\pi R_p(X)^3 \Pi^o_{el}}{A}, \qquad \alpha_x = 2\kappa R_p(x).$$

Tangential stress balance

$$-M_2\frac{\partial \Gamma}{\partial R} + M_3\frac{\partial}{\partial R}\left(\frac{1}{R}\frac{\partial (RV)}{\partial R}\right) - H\left(\frac{\partial P}{\partial R}\right) = 0, \qquad (6)$$

where $\Gamma = \Gamma/\Gamma_o$ is the dimensionless surfactant surface concentration, and V is the dimensionless surface velocity. The parameters M_2 and M_3 are given as

$$M_2 = \frac{E^o}{\sigma}, \qquad M_3 = \frac{\mu_{d+s}}{3\mu R_p(x)},$$

where E^o is the surface elasticity, and μ_{d+s} is the sum of the surface dilatational viscosity μ_d and the surface shear viscosity μ_s.

Surfactant surface mass balance

For an insoluble surfactant the surfactant mass balance is given by Fick's law as follows:

$$\frac{\partial \Gamma}{\partial X} + \frac{1}{R}\frac{\partial}{\partial R}(RV\Gamma) = \frac{M_4}{Ca_x}\frac{1}{R}\frac{\partial}{\partial R}\left(R\frac{\partial \Gamma}{\partial R}\right) + \frac{1}{R_p}\frac{dR_p}{dX}R\left(\frac{\partial \Gamma}{\partial R}\right), \qquad (7)$$

where the parameter M_4 is defined as

$$M_4 = \frac{3\mu D_s}{\sigma R_p(x)},$$

with D_s, the surfactant surface diffusivity.

The boundary conditions in terms of dimensionless variables are:

At $R = 0$:

Due to the natural symmetry of the system we have

$$\frac{\partial H}{\partial R} = 0$$

$$\frac{\partial P}{\partial R} = 0$$

$$\frac{\partial \Gamma}{\partial R} = 0$$

$$V = 0$$

At $R = 1$:

We assume that the interface forms a finite contact angle, independent of time

$$\frac{\partial H}{\partial R} = s.$$

Constant capillary pressure is assumed because in a realistic porous medium the grooves and channels permit liquid transport to equalize any local gradients in P_c. Thus it is expected that the capillary suction pressure exerted in the plateau borders is very close to that of the medium $P_{c,s}$.

$$P = -\frac{P_{c,s}}{P_o}.$$

Zero flux of the surfactant gives

$$\frac{\partial \Gamma}{\partial R} = 0$$

$$V = 0.$$

Dimensionless Parameters

Before we go into the numerical solution of the problem just defined, let us list the dimensionless parameters present in the governing equations.

From Eq. 2 we have the following parameters:

$$Ca_x = \frac{3\mu Q}{\pi\sigma L R_p(x)}, \quad \beta = \frac{1}{2}(a-1), \quad a = \frac{R_b}{R_t}.$$

The parameter β comes from the term $(1/R_p)(dR_p/dX)$ in Eq. 2, which is given as (using Eq. 1):

$$\frac{1}{R_p}\frac{dR_p}{dX} = \frac{\beta\pi\sin(\pi X)}{1+\beta[1-\cos(\pi X)]}.$$

Since this is a moving-boundary problem, the dimensionless parameters as they appear in the equations are dependent on axial location X in the pore. In order to study the effect of these parameters on the hydrodynamics of a foam film, we use the following axially independent counterparts of these parameters. Details of these derivations can be found elsewhere (Singh, 1996). Substituting $(1/R_p)(dR_p/dX)$ in Eq. 2 and dividing by β we can define a capillary number that accounts for the radial expansion of the lamella traversing the periodically constricted pore as follows:

$$Ca = Ca_x(x = L)\frac{2\beta}{a}.$$

The axially independent dimensionless parameters are then given as follows:

$$Ca = \frac{3\mu Q}{\pi\sigma R_b L}\left(1 - \frac{R_t}{R_b}\right), \qquad a$$

$$\theta = \frac{48\pi R_b^3 \Pi_{el}^o}{A}, \quad \alpha = 2\kappa R_b, \frac{\Pi_{el}^o R_b}{\sigma}, \quad M_2, M_3, M_4.$$

Here Ca, the capillary number, is the measure of the rate of radial expansion of the lamella, and $R_p(x)$ has been replaced by R_b in the expressions for M_3 and M_4.

Other dimensionless parameters appear in the boundary conditions and are given as

$$s, \qquad \frac{P_{c,s}R_b}{\sigma}.$$

The parameter s determines the geometry of the lamella and does not play any role in foam-film stability.

As pointed out in Singh (1996), parameters M_2, M_3, and M_4 can be grouped as follows:

$$N_\Gamma = \frac{M_2}{M_4}, \qquad N_\mu = M_3, \tag{8}$$

where N_Γ is the dimensionless elasticity number and N_μ is the dimensionless surface viscosity number (Singh, 1996; Singh et al., 1996). Further, it was observed that for both plane-parallel and dimpled films, the parameters N_μ and N_Γ interact in a linear additive manner and can be grouped into a single dimensionless parameter N_R as follows:

$$N_R = N_\mu + 0.27N_\Gamma. \tag{9}$$

We anticipate that same is true for the present situation, that is, that key aspects of film behavior depend on N_R and not on N_μ and N_Γ individually.

We know that a static foam film is unstable at a capillary pressure (P_{cr}) that equals the maximum in the disjoining pressure curve $\Pi_{\max}$ (see Figure B1). Further, $\Pi_{\max}$ depends on surfactant and electrolyte concentration, that is, the parameters θ, α, and $(\Pi_{el}^o R_b)/\sigma$. Thus the parameter $P_{cr} = \Pi_{\max}[\theta, \alpha, (\Pi_{el}^o R_b)/\sigma]$ is defined by these three parameters. For our study we group these parameters and $(P_{c,s}R_b)/\sigma$ into a single dimensionless parameter m such that

$$m = \frac{P_{c,s}}{P_{cr}(=\Pi_{\max})}. \tag{10}$$

This parameter is the ratio of the capillary pressure in the medium $P_{c,s}$ for a foam film to the critical capillary pressure P_{cr} of a static foam film. Thus for values of $m \ll 1$, the foam film will be stable.

Finally, we have four most important dimensionless parameters that affect the hydrodynamics of a foam film in a porous medium:

$$Ca, \qquad a, \qquad N_R, \qquad m.$$

Note that some dimensionless parameters appearing in the governing equations and boundary conditions, for example, θ, α, do have effects on lamella behavior beyond influencing values of the key parameters just mentioned. These additional effects have not been neglected in our solution, but they are considered secondary and so are not investigated explicitly.

Initial Conditions

The initial conditions for the film thickness are based on the capillary pressure of the medium $P_{c,s}$. For $P_{c,s} > P_{\text{trans}}$, where

$$P_{\text{trans}} = \frac{2\sigma}{R_t},$$

there is a lamella at the pore throat, and for $P_{c,s} < P_{\text{trans}}$ we have a slug of liquid—a lens—at the pore throat. Further, we make sure that $P_{c,s}$ is greater than σ/R_t, which is the condition for snap off (Ransohoff and Radke, 1986).

Lens at the pore throat

If the capillary pressure of the porous medium $P_{c,s}$ is less than the transition pressure P_{trans}, then the initial profile at the pore throat is that of a pair of hemispherical menisci of radius $R_s = (2\sigma/P_{c,s})$ separated by a distance $2h_i$. The initial half thickness is calculated from geometric consideration as:

$$h_i = \frac{L}{\pi}\cos^{-1}\left[1 - 2\frac{(R_s/R_t - 1)}{(R_b/R_t - 1)}\right] - R_s. \tag{11}$$

We will not be considering this case in our study.

Lamella at the pore throat

For $P_{c,s} > P_{\text{trans}}$, we have a lamella at the pore throat. Under conditions of static equilibrium this implies that the thickness of the film is governed by the disjoining pressure isotherm $\Pi = \Pi(h)$.

Determination of the initial film profile

The initial film profile in this case is that of a flat film of thickness h_i and radius R_f, associated with a meniscus with a radius of curvature corresponding to the capillary pressure in the medium (Figure 2).

At the equilibrium film thickness the capillary pressure exerted in the plateau borders equals the disjoining pressure in the film, hence $h_i = h_{\text{eq}}$, which is given as

$$\Pi(h_{\text{eq}}) = P_{c,s}.$$

Thus for a given $P_{c,s}$ and a given disjoining pressure isotherm (Eq. B1) the equilibrium thickness is determined by solving the preceding nonlinear equation using a hybrid algorithm of Newton–Raphson and the bisection method. Figure B1 (see Appendix B) shows that in general three distinct roots are

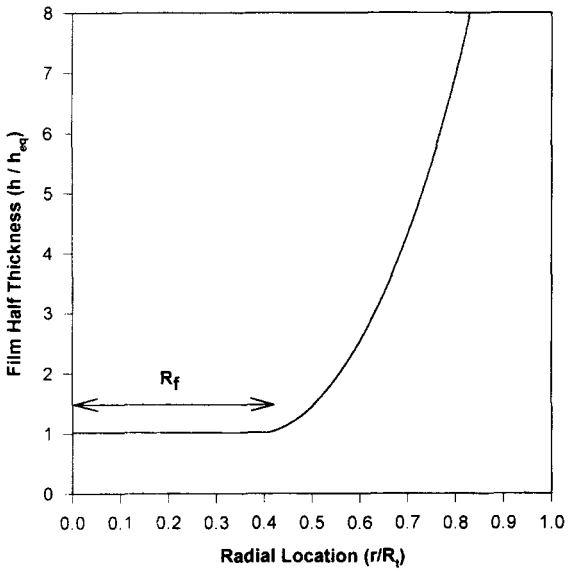

Figure 2. Initial film-thickness profile of a foam lamella/film in a pore.

possible, but the root of interest is the one of maximum thickness, as the middle root is unstable and the minimum root corresponds to a Newton black film that is beyond our region of interest.

The Young–Laplace equation is assumed for the thickness profile in the meniscus region. The initial lamella thickness profile is then computed numerically by solving the Young–Laplace equation using a fourth-order Runge-Kutta method.

Numerical Method

With the preceding initial conditions and the respective boundary conditions the set of partial differential equations (Eqs. 2–7) is solved numerically by a finite difference method. One has to take note that this is a moving boundary problem. We used the so-called "semi-implicit" procedure, where the spatial differences for the flux terms were evaluated with a linear approximation to the new axial level using unknown values of the dependent variable H. The governing equations are transformed into a system of linear equations, where the unknowns are the change in film half thickness at each grid block. Upstream weighting is used for convective terms. The resulting equations are pentadiagonal in thickness H and block tridiagonal in V and Γ. The system was solved using a lower and upper (LU) decomposition and then an upper and lower back substitution.

We adopted an automatic axial step-size selection such that the maximum relative change in H and R_p per axial step did not exceed a given value of 5% and 0.5%, respectively.

Results and Discussion

As stated earlier, foam stability in porous media depends on how film thickness changes as the lamella traverses the pore, especially as it expands in going from a pore throat to a pore body. Let us clarify the difference between "stretching" and "expansion." The lamella, as it goes from a small pore (pore throat) to a larger pore (pore body), undergoes an expansion, as it conforms to the pore wall. On the other hand, if the lamella is very mobile such that it thins uniformly, we say it is stretching. Thus stretching is a subset of expansion, and the terms are not equivalent. The expansion in turn depends both on the pore aspect ratio a, which determines the amount of expansion, and on pore length L and flow rate Q, which determine the rate of expansion.

The translating foam lamella, which is opposed by surface elastic forces and surface viscous traction, drains due to capillary suction exerted at the plateau borders. On the other hand, the disjoining pressure, as the name implies, tends to fill the lamella to the equilibrium thickness. Further, the relative effect of these forces tending to drain/fill the lamella depends on the rate at which the lamella expands, that is, on the pore geometry and the flow rate. For a given pore geometry, medium capillary pressure, disjoining pressure isotherm, and flow rate, if the film thins down to the critical thickness (h_{cr}, Figure B1) at any point, it becomes unstable and breaks. Foam stability in a porous medium thus depends on the complex interplay of the aforementioned parameters.

Previous researchers (Jiménez and Radke, 1989) have used a plane-parallel model [$(\partial H/\partial R) = 0$] to examine the effects of flow rate, capillary pressure, and aspect ratio on the stability of a foam film traversing a periodically constricted sinusoidal pore. Although they have used the Reynolds model for film thinning with a correction factor (α_s) for a mobile film, nearly all their numerical results are for a rigid (immobile, $\alpha_s = 0$) film. In our analysis, governing equations along with the boundary conditions (the second section) have been solved with no additional approximations, but as mentioned in the third section, we present our analysis as a function of the key dimensionless parameters, namely Ca, N_R, a, and m. The values used in our simulations are based on the typical values reported by Chambers and Radke (1992) in their experiments on foam flow. They report frontal advance rates (interstitial velocities) ranging from 30 m/day to 300 m/d. Typical widths of pore bodies ranged from 150 μm to 300 μm, while the widths of pore throats varied between 25 and 125 μm. Similar data have been reported by Rossen (1995). Table 1 lists some of the values used in our study and the corresponding dimensionless parameter values.

Immobile film

We first present the results for an immobile (rigid) film (i.e., film with tangentially inextensible surfaces) as it moves down the pore. We found earlier in the study of hydrodynamics of stationary mobile foam films (Singh et al., 1996) that the parameter N_R determines the mobility of the film, and that for N_R sufficiently large ($> 10^4$) the film is immobile. Hence the immobile film simulations were carried out at high values of N_R. As mentioned earlier an initial lamella/film profile is calculated under given conditions and the simulator is allowed to move the lamella through a series of pore-throat

Table 1. Parameter Values

u(m/d)	Q(m^3/s)	R_t(μm)	R_b(μm)	L(μm)	$P_{c,s}$(kPa)	Ca
180	2.6×10^{-10}	100	200	100	7.0	2×10^{-4}

and pore-body configurations. The results are recorded when a periodic change in behavior of lamella thickness (as it goes from throat to body) is observed. It is seen that periodicity is achieved sooner (≈ 10 pore lengths) at low capillary number (Ca), while at high Ca it may take around 600 pore lengths.

Film thickness changes were computed at different Ca for a given disjoining pressure isotherm (Figure B1), pore geometry, and constant medium capillary pressure $P_{c,s}$. At low capillary numbers Ca, as the lamella moves from pore throat to pore body one can see that (Figure 3) the film expands at a constant thickness (i.e., the equilibrium thickness). This is evident from Eq. 2, since at low capillary number the film thickness is governed by the disjoining pressure Π.

Contrary to the results of Jiménez and Radke (1989), we observe that at high capillary number Ca the film expands by entraining liquid as it moves from a pore throat to a pore body rather than by stretching and thinning, which cannot occur at high N_R because tangential motion at the surfaces is precluded. Simulated film half-thickness profiles, illustrated in Figure 4, show development of a rim that increases the pressure gradient for outward flow of liquid. The minimum in thickness between the rim and meniscus decreases as outward motion of the film slows in the latter part of the expansion. Our calculations show that it also increases with increasing Ca at a given point during the expansion.

Explanation for this behavior can be sought by considering Bretherton's (1961) asymptotic solution for thickness of a long advancing bubble in a capillary tube. Figure 5 shows the schematic underlying the mathematical similarity of the two solutions. This behavior is also closely related to other situations that have been studied previously, namely, the formation of a soap film by withdrawal of a vertically oriented frame from a surfactant solution (Mysels et al., 1959), and flow of bulk foams of high gas content (Schwartz and Princen, 1987; Reinelt and Kraynik, 1990). In all these cases scaling of the equations of motion shows that the film thickness is proportional to $Ca^{2/3}$.

In Bretherton's (1961) analysis U_{Br} is the axial velocity of the bubble. In the present analysis U is the rate at which the lamella is expanding. Bretherton showed that the film thickness h_{Br} laid down by this advancing bubble is directly pro-

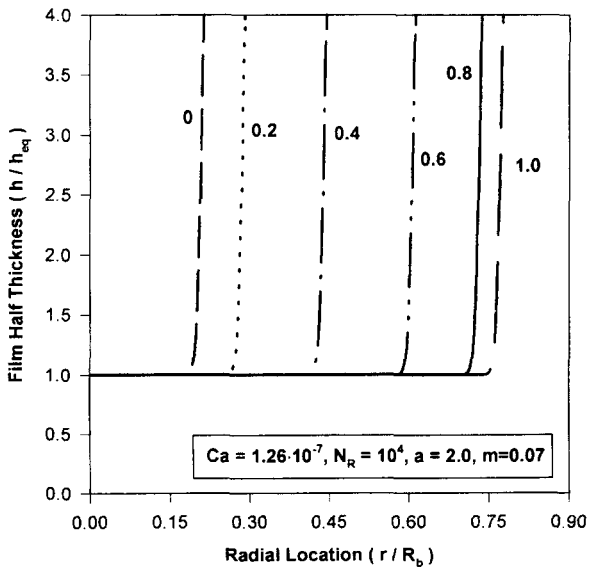

Figure 3. Film half-thickness profiles as the lamella moves from pore throat to pore body for low capillary number *Ca*, $m = 0.07$, $a = 2$.

Axial locations have been posted.

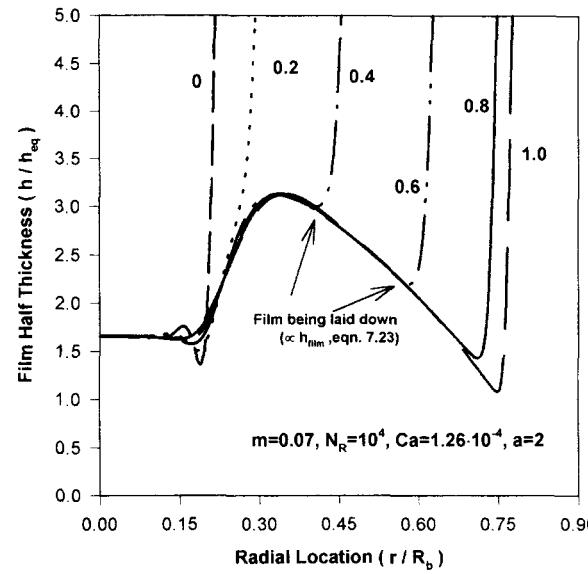

Figure 4. Film half-thickness profiles as the lamella moves from pore throat to pore body for medium capillary number *Ca*, $m = 0.07$, $a = 2$.

Axial locations have been posted.

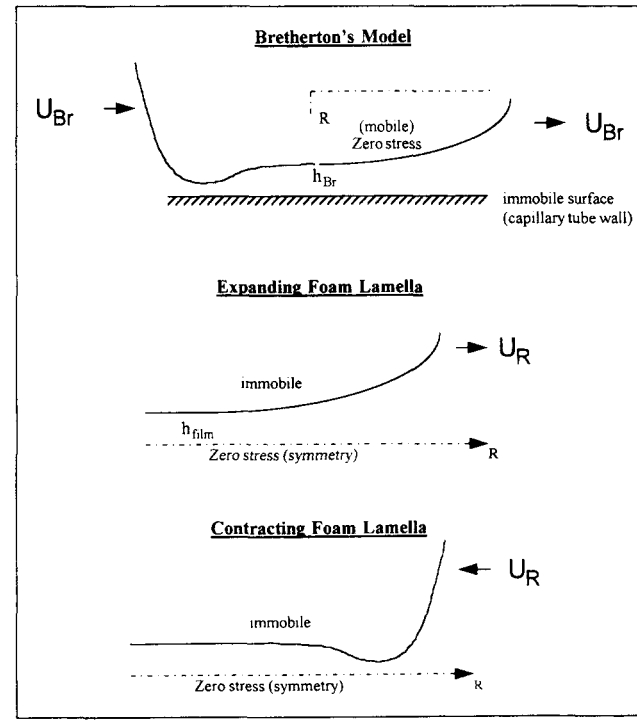

Figure 5. Mathematical similarity of Bretherton's analysis and expanding foam lamella problem.

portional to the capillary number (flow velocity) raised to the 2/3 power and is given as

$$h_{Br} = 0.643 R_{Br}\left(\frac{3\mu U_{Br}}{\sigma}\right)^{2/3}, \qquad (12)$$

where R_{Br} is the capillary radius and also the radius of curvature of the meniscus. Realizing the similarity in the analyses, we can write the rate of expansion of the lamella as

$$U_R(x) = \frac{dR_p}{dt} = \frac{dR_p}{dx}\frac{Q}{\pi R_p^2}.$$

Indeed the thickness of the film laid down as predicted by our simulations was found to be approximately proportional to Bretherton's expression (Eq. 12) and is given as follows:

$$h_{\text{film}} = 1.44 R_s\left(\frac{3\mu U_R}{\sigma}\right)^{2/3}, \qquad (13)$$

where R_s is the radius of curvature of the meniscus and is given as $(2\sigma/P_{c,s})$. Figure 6 compares the film thickness predicted by our simulations to that predicted by Eq. 13. It shows that for a lamella with immobile surfaces, as the capillary number (flow rate Q) increases, the film entrains liquid and becomes thicker contrary to the thinning found by Jiménez and Radke (1989) based on their plane-parallel model. Thus, film thickness as the lamella expands, has the same dependence on instantaneous capillary number as that predicted by the Bretherton theory for thickness at front of bubble moving in a capillary tube. Further, it is seen that film thickness profiles (Figure 7) as the lamella moves from pore body to pore throat are similar to those observed at the back of a bubble moving in a capillary tube.

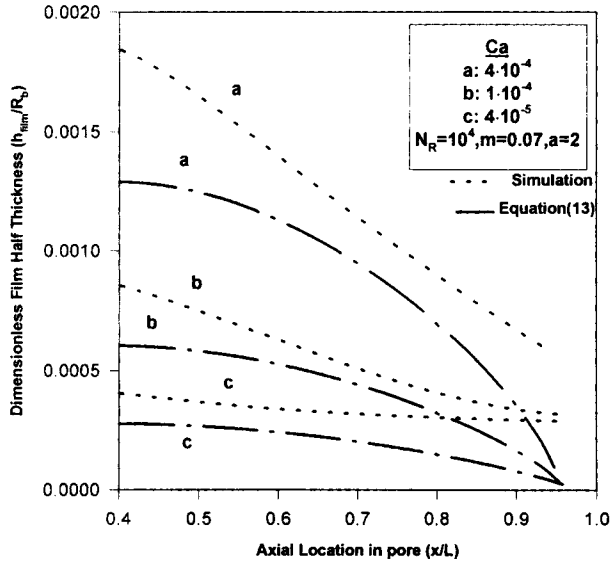

Figure 6. Comparison of film thickness predicted by numerical simulation to Bretherton-type thickness (Eq. 13).

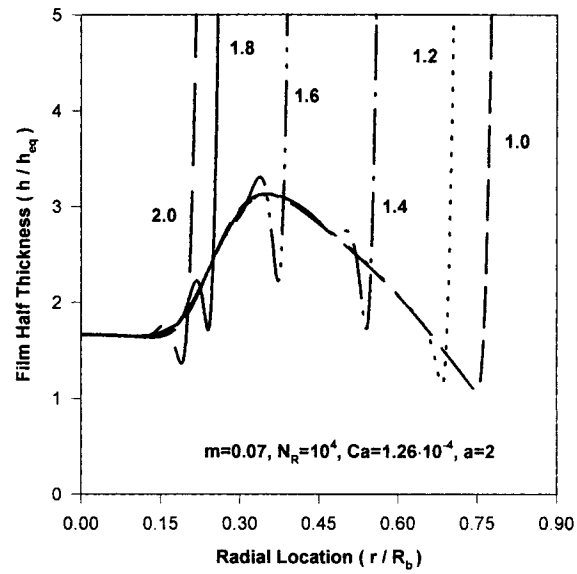

Figure 7. Film half-thickness profiles as the lamella moves from pore body to pore throat for medium capillary number Ca, $m = 0.07$, $a = 2$.
Axial locations have been posted.

Proceeding on the earlier idea of axially independent counterparts of parameters, we now present a characteristic film thickness $\bar{h}_{\text{film}}$ as a function of an average rate of lamella expansion $\bar{U}_R$ independent of the axial location x in the pore.

From the definition of U_R we thus have

$$\frac{3\mu\bar{U}_R}{\sigma} \approx \frac{3\mu Q}{\pi\sigma R_b}\frac{1}{R_b}\frac{(R_b - R_t)}{L}.$$

A close look reveals that this is the capillary number Ca as defined in the previous section. Substituting the preceding expression in Eq. 13 gives

$$\bar{h}_{\text{film}} = 1.44 R_s Ca^{2/3}. \qquad (14)$$

We observe from these simulations that at low Ca, the film thickness is governed by Π, while the Bretherton effect becomes dominant at high values of Ca. In fact we can quantitatively describe the capillary number at which the transition from disjoining pressure controlled to the Bretherton effect occurs, through the following equation

$$\frac{h_{\text{eq}}}{R_s} = \frac{\bar{h}_{\text{film}}}{R_s}.$$

This represents the intersection of the equilibrium thickness line with the curve for Eq. 14.

Substituting from Eq. 14, we have

$$Ca_{\text{tran}} = \left(\frac{h_{\text{eq}}}{1.44 R_s}\right)^{3/2}.$$

For the medium capillary pressure $P_{c,s}$ and the disjoining pressure isotherm used, we have $Ca_{\text{trans}} = 7.54 \cdot 10^{-5}$. This is about what we see from the results of our simulations in Figure 8, which is a contour plot of $h_{\min}/h_{\text{eq}}$ for various regimes of the capillary number Ca and the surfactant number N_R. Here $h_{\min}$ is the minimum thickness the lamella attains as it traverses the sinusoidal pore. Note that higher values of Ca where the Bretherton effect is important are achieved for realistic conditions (Table 1). Figure 8 shows that for high N_R (immobile film) the ratio $h_{\min}/h_{\text{eq}}$ increases with capillary number Ca. In the next subsection we discuss the results of our simulations for low values of N_R (mobile film) as seen on the contour plot (Figure 8).

Mobile film

The contour plot Figure 8 shows a remarkable effect of surface mobility (N_R) on the hydrodynamics of the lamella. For low values of N_R we see that the ratio $h_{\min}/h_{\text{eq}}$ decreases as the capillary number (or flow rate Q) increases. No unstable regions are observed since the medium capillary pressure $P_{c,s}$ is low ($m = 0.07$) and hence the film never thins down to the critical thickness $h_{c,r}$ (Figure B1). The effect of increasing Ca on foam stability is in direct contrast to the behavior seen in the preceding subsection for high N_R (immobile film). It is observed that for low N_R (mobile films) the dimensionless minimum film half thickness $h_{\min}/h_{\text{eq}}$ decreases with increasing capillary number Ca until it reaches a minimum for fixed N_R and then starts to increase with Ca as entrainment (Bretherton effect) sets in.

The profiles of film half thickness h as a lamella moves from pore throat to pore body for low N_R can be seen in Figure 9. As shown the film stretches and thins down even below its equilibrium thickness. At high enough Ca or at a high dimensionless capillary pressure m the lamella could

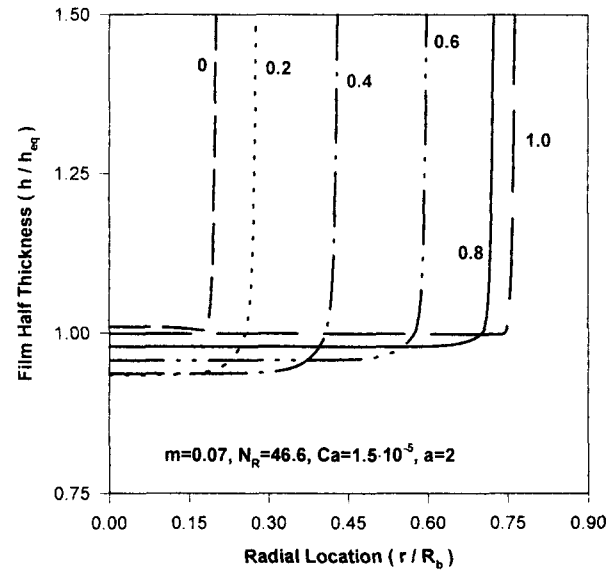

Figure 9. Film half-thickness profiles at high *Ca* and low $N_R = 46.6$ as the lamella moves from pore throat to pore body, $m = 0.07$, $a = 2$.

Axial locations have been posted

thus thin down to its critical thickness and break. Figure 10 shows profiles for the previous case as the lamella goes from pore body to pore throat. The dimpling observed is similar to the waviness in the film observed at the back of a bubble moving in a capillary tube.

The film-stretching behavior just described is in qualitative agreement with the results of Jiménez and Radke (1989) who assumed the lamella to be plane parallel, that is, the film stretches and consequently thins as it goes from pore throat to pore body. This implies that a plane-parallel model is a

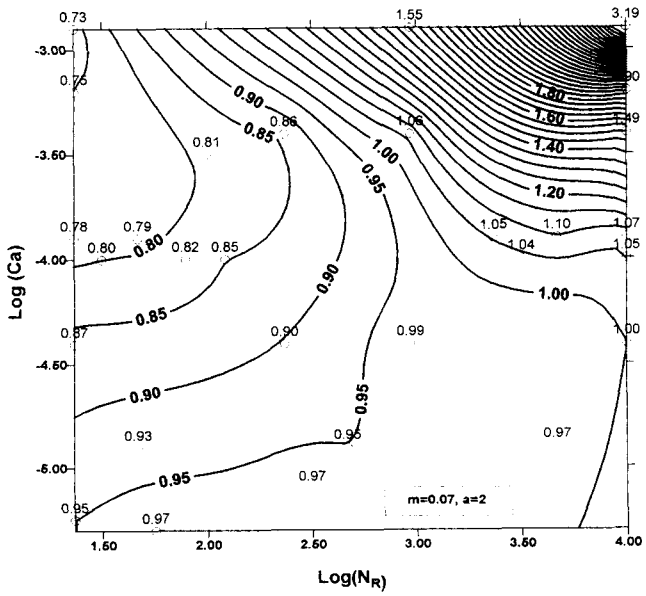

Figure 8. Contours of dimensionless minimum film half thickness ($h_{\min}/h_{\text{eq}}$) as a function of capillary number *Ca* and surfactant number N_R, for $m = 0.07$ and $a = 2$.

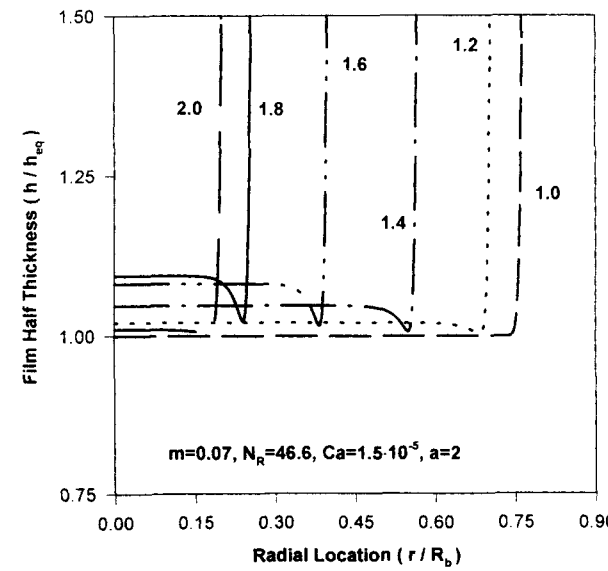

Figure 10. Film half-thickness profiles at high *Ca* and low $N_R = 46.6$ as the lamella moves from pore body to pore throat, $m = 0.07$, $a = 2$.

Axial locations have been posted.

good approximation if the lamella is highly mobile (rather than an immobile film, the reason being that the plane-parallel model is unable to account for the entrainment effect (Figure 4)). The dimensionless minimum film half thickness (h_{min}/h_{eq}) as predicted by our simulations has been compared with the results of Jiménez and Radke (1989) in Figure 11. This figure illustrates that for a highly mobile film (low N_R), reasonable agreement is achieved between the two models. Quantitatively, one expects both results to match in the limit of vanishing N_R, that is, for an infinitely mobile film that will stretch/squeeze as a plane-parallel film. Nevertheless our analysis is more complete and hence better for quantitative work.

Thus from our simulations we see that, depending on the capillary number Ca and the surfactant number N_R, we could be in completely different regimes of lamella hydrodynamics. It was observed that the lamella is susceptible to breaking at low values of N_R and high capillary number Ca, while at high values of N_R it becomes more stable with increasing Ca due to the entrainment effect.

We now discuss the implications of the results just presented, especially those of Figure 8. The dependence of film thickness on N_R and Ca suggests two different regimes for the stability of moving and stationary lamellae for foam flowing at the limiting capillary pressure. (1) When N_R is large, moving lamellae (larger Ca) may be more stable than stationary lamellae (smaller Ca). If this is the case, moving lamellae trains will switch paths as stationary lamellae rupture and new paths of least resistance appear. This may be the preferred mode of foam flow when it is desired to contact as much of the porous medium as possible with flowing discontinuous-gas foam. (2) When N_R is small, the stationary lamellae will be more stable than the moving lamellae. In this case, the foam breakage may be catastrophic. The rupture of moving lamellae in a train will reduce the resistance of the train. The reduced resistance will lead to a higher velocity and thus higher Ca. This higher Ca will further destabilize the lamellae. In this case, the foam, if it is flowing, may be a continuous-gas foam.

Now that we have a good insight into lamella hydrodynamics, let us explain the dependence of limiting medium capillary pressure on the capillary number Ca (flow rate Q) with regard to foam stability in porous media.

For a given disjoining pressure isotherm, surface rheological properties (i.e., surfactant number N_R), pore geometry (aspect ratio a), and flow rate Q (capillary number Ca) we record the film-thickness profiles (as a lamella traverses pore throats and bodies) for varying medium capillary pressures. The capillary pressure at which the film thins down to the critical thickness and breaks is termed as the limiting capillary pressure $P^*_{c,s}$ (i.e., $m = m^*$). Figure 12 illustrates the results of various simulations carried out for different sets of Ca and N_R. For a given Ca, N_R and fixed disjoining pressure isotherm Π and aspect ratio we calculated the lamella thickness as it traverses the pore for different values of dimensionless capillary pressure m. The dimensionless limiting capillary pressure m^* was identified as the pressure at which the lamella thinned down to the critical thickness h_{cr} corresponding to a maximum in the disjoining pressure isotherm Π_{max} (e.g., see Figure B1). A bisection-type approach was used to zero in on the limiting capillary pressure value. The effect of flow rate Q (capillary number Ca) on the dimensionless limiting capillary pressure m^* ($= P^*_{c,s}/P_{cr}$) has been shown at different values of the surfactant number N_R. Note that such an instability can occur under realistic conditions (Table 1). The surfactant formulation, that is, the electrolyte concentration, surfactant charge, Hamaker constant, and so on, also affects the stability of the lamella, that is, it may be unstable even at low values of m and at comparable Ca for high electrolyte concentration or large Hamaker constant. Figure 12 shows that the experimentally observed behavior of decreasing m^* with increasing Ca (Khatib et al., 1988) is characteristic of lamellae with high mobility (low N_R). Fur-

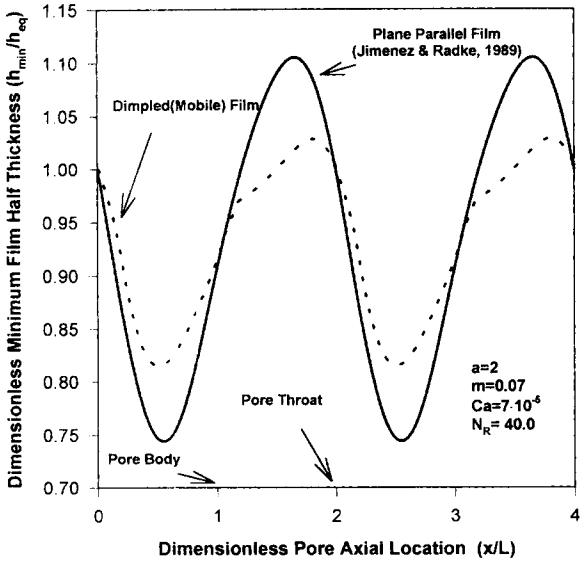

Figure 11. Comparison of film thickness between our simulation and Jiménez and Radke (1989) as the lamella moves from pore throat to pore body, for low N_R.

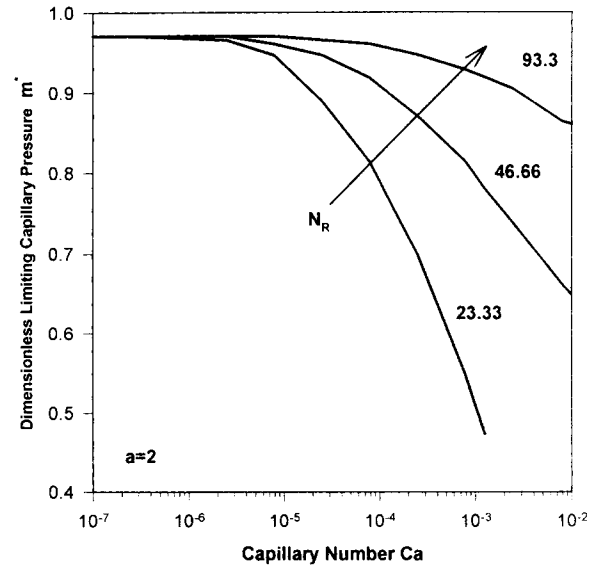

Figure 12. Dimensionless limiting capillary pressure m^* as a function of capillary number Ca at different values of surfactant number N_R.

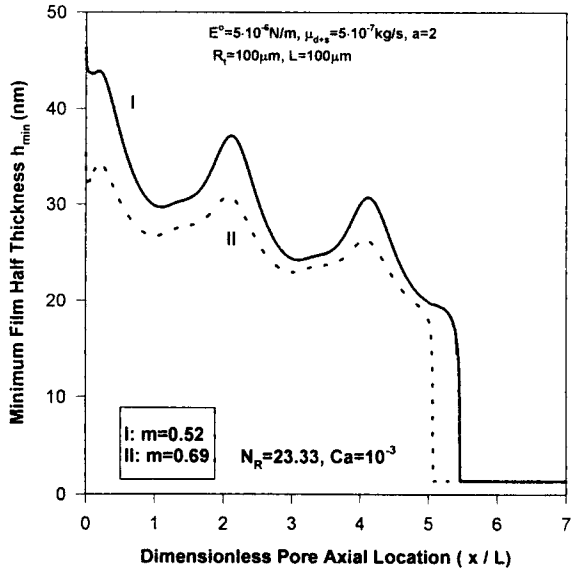

Figure 13. Dimensionless minimum film half thickness h_{min}/h_{eq} as the lamella traverses the pore for $m \geq m^*$.

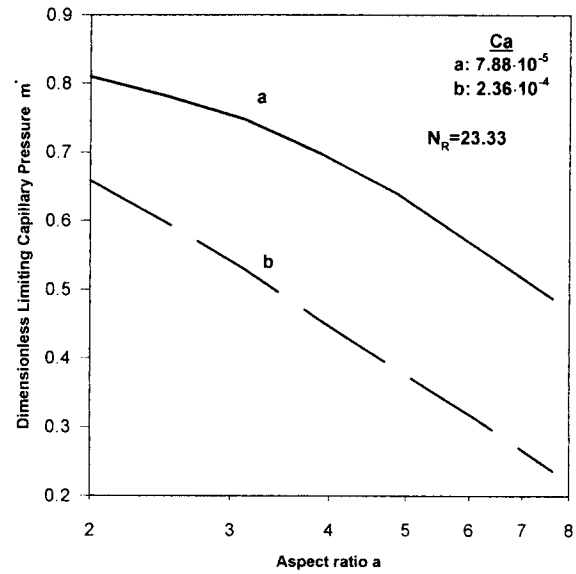

Figure 15. Effect of pore aspect ratio a on dimensionless limiting capillary pressure m^* at different capillary numbers Ca.

ther, this dependence of m^* on Ca decreases as the film mobility decreases (i.e., N_R increases), and for an immobile film m^* is independent of the capillary number Ca.

Figure 13 illustrates the evolution of minimum film half thickness for a couple of conditions presented in Figure 12. It shows that for $m \geq m^*$ the film stretches and thins down to its critical thickness, where it may become unstable and break. A contour plot of h_{min}/h_{eq} for a large value of m such that the preceding instability occurs for certain regions of the parameters Ca and N_R is presented in Figure 14 (the disjoining pressure isotherm parameters, e.g., the electrolyte concentration C_{el} and the Hamaker constant A were appropriately adjusted). It shows that for low values of N_R and high capillary number Ca the foam lamella is unstable, that is, the ratio h_{min}/h_{eq} drops below 0.7 (corresponding to the critical thickness h_{cr}) and hence this region is not suitable for operation in a foam process aimed at reducing gas mobility.

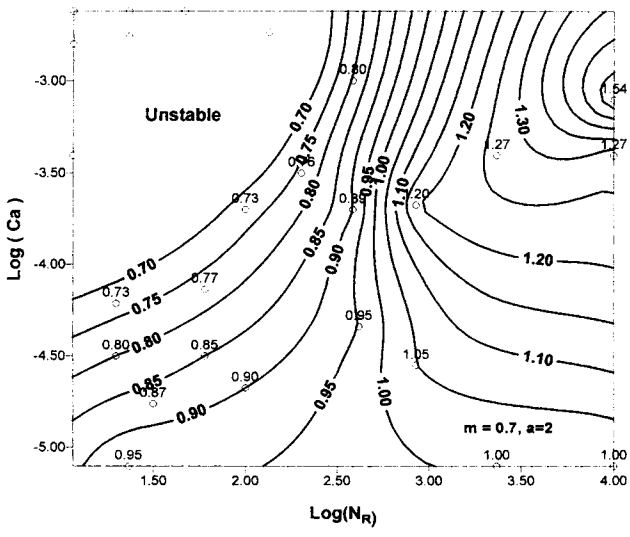

Figure 14. Contours of dimensionless minimum film half thickness h_{min}/h_{eq} at a high capillary pressure in the porous medium, $m = 0.7$; $C_{ei} = 2.5\times10^{-4}$, $A = 8\times10^{-18}$ J.

Figure 15 shows the effect of aspect ratio a on foam stability (dimensionless limiting capillary pressure m^*) for different values of Ca, at low N_R. As expected higher a leads to increased stretching of a lamella as it goes from pore throat to pore body, leading to a more unstable foam. A given porous medium will have a distribution of pore throat and pore body sizes. Hence for a given flow rate (capillary number Ca) and capillary pressure the lamella will break at locations where the aspect ratio a exceeds the value shown in Figure 15. These sites are called termination sites. Although this article addresses the problem of a periodically constricted pore with a constant aspect ratio, one could use the preceding simulator to study foam-film hydrodynamics in a more heterogenous medium where the aspect ratio between subsequent pore throats and bodies is different.

Conclusions

1. The film hydrodynamics in porous media strongly depend on the parameters Ca, the capillary number, and N_R, the surfactant number. Based on the values of these parameters, the behavior of the lamella, as it goes from pore throat to pore body, can be divided into different regimes.

2a. For large values of N_R (immobile film) the ratio h_{min}/h_{eq} increases with increasing capillary number Ca (or flow rate) indicative of the Bretherton or entrainment effect. The capillary number above which this effect becomes dominant has been quantified.

2b. For low values of N_R the behavior is opposite, that is, the ratio h_{min}/h_{eq} initially decreases with increasing capillary number Ca (or flow rate). Also seen is that h_{min}/h_{eq} goes

through a minimum with increasing Ca and starts to increase due to the entrainment effect setting in.

3a. At low N_R (mobile film) the lamella may thin down to its critical thickness and break. Thus the experimentally observed dependence of dimensionless limiting capillary pressure, m^*, on the flow rate Ca (capillary number) with respect to foam stability is accounted for. This is in agreement with the results of Jiménez and Radke (1989).

3b. For large N_R (immobile film) it is shown that contrary to Jiménez and Radke (1989), whose analysis does not include the entrainment effect, the film will not break unless the capillary pressure $P_{c,s}$ corresponds to the maximum in disjoining pressure isotherm Π_{max}.

4. The effect of the pore shape (aspect ratio a) on the foam stability in terms of the limiting capillary pressure of the porous medium has been presented. As expected it is seen that large pore-body-to-pore-throat ratios are detrimental to foam stability. Such sites in a porous medium are known as termination sites for foam films.

Acknowledgment

This work was partially supported by Exxon Production Research, Houston. The authors wish to thank Dr. G. F. Teletzke, Exxon Production Research. for helpful comments.

Notation

H = dimensionless-film half thickness
P = dimensionless pressure in foam lamella
$P_{c,s}$ = capillary pressure in porous medium
R = dimensionless radial location
v_r^s = radial component of surface velocity
β = shape parameter for pore radius
Γ_o = initial surfactant surface concentration
μ = bulk shear viscosity
σ = thermodynamic surface tension
Π_{sr} = steric component of disjoining pressure

Subscripts

p = pore variable
x = axially dependent

Literature Cited

Bretherton, F. P., "The Motion of Long Bubbles in Tubes," *J. Fluid Mech.*, **10**, 166 (1962).

Chambers, K. T., and C. J. Radke, "Capillary Phenomena in Foam Flow Through Porous Media," *Interfacial Phenomena in Petroleum Recovery*, N. R. Morrow, ed., Vol. 36, Surfactant Science Series, Marcel Dekker, New York, p. 191 (1992).

Falls, A. H., G. J. Hirasaki, T. A. Patzek, P. A. Gauglitz, D. D. Miller, and T. Ratulowski, "Development of a Mechanistic Foam Simulator: The Population Balance and Generation by Snap-Off," *SPE Reserv. Eng.*, **3**, 884 (1988).

Hirasaki, G. J., C. A. Miller, R. Szafranski, J. B. Lawson, and N. Akiya, "Surfactant/Foam Processes for Aquifer Remediation," SPE Symp. Oilfield Chem., Houston (1997).

Ivanov, I. B., "Effect of Surface Mobility on the Dynamic Behavior of Thin Liquid Films," *Pure Appl. Chem.*, **52**, 1241 (1980).

Jiménez, A. J., and C. J. Radke, "Dynamic Stability of Foam Lamellae Flowing through a Periodically Constricted Pore," *Oil Field Chemistry: Enhanced Oil Recovery Production Simulation*, J. K. Borchardt and T. F. Yen, eds., ACS Symp. Ser. 396, Amer. Chem. Soc., Washington, DC (1989).

Joye, J. L., C. A. Miller, and G. J. Hirasaki, "Dimple Formation and Behavior during Axisymmetrical Foam Film Drainage," *Langmuir*, **8**(12), 3083 (1992).

Khatib, Z. I., G. J. Hirasaki, and A. H. Falls, "Effects of Capillary Pressure on Coalescence and Phase Mobilities in Foams Flowing through Porous Media," *SPE Reserv. Eng.*, **3**, 919 (1988).

Kovscek, A. R., and C. J. Radke, "Fundamentals of Foam Transport in Porous Media," *Foams: Fundamentals and Applications*, L. L. Schramm, ed., ACS Symposium Ser. 242, Amer. Chem. Soc., Washington, DC (1994).

Mysels, K. J., K. Shinoda, and S. Frankel, *Soap Films: Studies of Their Thinning*, Pergamon, New York (1959).

Nutt, C. W., R. W. Burly, D. M. Anwer Rajah, and J. T. Polichronopolis, "Foam Generation in Porous Media," *Int. J. Eng. Fluid Mech.*, **5**(3), 373 (1992).

Ransohoff, T. C., and C. J. Radke, "Mechanisms of Foam Generation in Glass Bead Packs," *SPE Reserv. Eng.*, Vol. 3, 619 (1988).

Reinelt, D. A., and A. M. Kraynik, "On the Shearing Flow of Foams and Concentrated Emulsions," *J. Fluid Mech.*, **215**, 431 (1990).

Reynolds, O., *Philos. Trans. R. Soc. London*, **177**, 157 (1886).

Rossen, W. R., "Foams in Enhanced Oil Recovery," *Foams: Theory, Measurements and Applications*, R. K. Prud'homme and Saad A. Khan, eds., Surfactant Science Series, Vol. 57, Dekker, New York (1995).

Schwartz, L. W., and H. M. Princen, "A Theory of Extensional Viscosity for Flowing Foams and Concentrated Emulsions," *J. Colloid Interf. Sci.*, **118**, 201 (1987).

Singh, G., PhD Thesis, Rice Univ., Houston (1996).

Singh, G., G. J. Hirasaki, and C. A. Miller, "Effect of Material Properties on the Drainage of Symmetric, Plane Parallel, Mobile Foam Films," *J. Colloid Interf. Sci.*, **184**, 92 (1996).

Appendix A: Derivation of Governing Equations

The film-thickness equation (Eq. 2) is nothing but an integrated form of the continuity equation (Singh, 1996), and is given as

$$\frac{\partial h}{\partial t} = -\frac{1}{r}\frac{\partial}{\partial r}(rhv_r^s) + \frac{1}{3\mu}\frac{1}{r}\frac{\partial}{\partial r}\left[rh^3\left(\frac{\partial p}{\partial r}\right)\right] \qquad \text{(A1)}$$

Since the foam film/lamella is translating in the pore, it also depends on the axial location x in addition to the variables t (time) and r (radial location). But there exists a one-to-one correspondence between the axial location x and the time t through the local interstitial velocity $v(x)$.

Thus replacing t by x in Eq. A1, we make Eq. A1 dimensionless, using $R_p(x)$ as the characteristic radial length. This step has to be performed with caution, as now $R = r/R_p$ is a function of the axial location x, which means we need to account for this in the partial derivatives ($\partial h/\partial x$). Thus, we have

$$\frac{\partial h}{\partial t} = \left(\frac{\partial h}{\partial x}\right)_r \frac{\partial x}{\partial t} = \left(\frac{\partial h}{\partial x}\right)_r \frac{Q}{\pi R_p^2(x)}.$$

Note that for

$$h = h(x,r) = h[x, R(x,r)]$$

we have

$$\left(\frac{\partial h}{\partial x}\right)_r = \left(\frac{\partial h}{\partial x}\right)_R - R\left(\frac{\partial h}{\partial R}\right)_x \frac{1}{R_p}\frac{dR_p}{dx}.$$

Converting Eq. A1 to dimensionless form by replacing x with $X = x/L$, r with $R = R(x,r)$, and h with $H = h/R_p(x)$, and realizing that

$$\left(\frac{\partial h}{\partial x}\right)_R = R_p\left(\frac{\partial H}{\partial x}\right)_R + H\frac{dR_p}{dx},$$

we have

$$Ca_x\frac{\partial H}{\partial X} + Ca_x H\left(\frac{1}{R_p}\frac{dR_p}{dX}\right) - R\left(\frac{\partial H}{\partial R}\right)\frac{1}{R_p}\frac{dR_p}{dX}Ca_x = -\frac{v_o 3\mu}{\sigma}\frac{1}{R}\frac{\partial}{\partial R}(RVH) + \frac{1}{R}\frac{\partial}{\partial R}\left(RH^3\frac{\partial P}{\partial R}\right), \quad \text{(A2)}$$

where v_o is the characteristic surface velocity. Using $v_o = \sigma/3\mu$, and dividing through by Ca_x, we get Eq. 2 as the governing equation for lamella thickness, as it translates in a periodically constricted sinusoidal pore.

Similar procedures are followed in making the other equations dimensionless, namely the surfactant surface mass balance.

Appendix B: Disjoining Pressure Isotherm

The disjoining pressure Π is the additional pressure that the film exerts as the film/lamella is thinned. This pressure (when positive) tends to disjoin the two interfaces. When the disjoining pressure is negative, it tends to contract the lamella.

It is a sum of three different terms:

$$\Pi = \Pi_{vdW} + \Pi_{el} + \Pi_{sr}, \quad \text{(B1)}$$

where Π_{vdW} is the van der Waals attraction term and is given as:

$$\Pi_{vdW} = -\frac{A}{48\pi h^3},$$

where A is the Hamaker constant. Π_{el} is the pressure due to the electrostatic repulsion, and can be expressed as

$$\Pi_{el} = 64nkT\phi^2 e^{-2\kappa(h-\delta)}$$

This can be written as

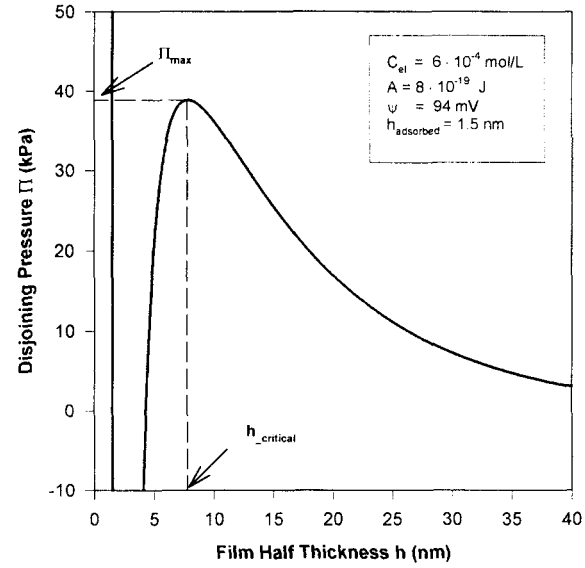

Figure B1. Disjoining pressure Π as a function of film half thickness *h*.

$$\Pi_{el} = \Pi_{el}^{o} e^{-2\kappa(h-\delta)}$$

$$\phi = \tanh\left(\frac{ze\psi}{4kT}\right)$$

$$\kappa^{-1} = (2e^2z^2n/\epsilon kT)^{-1/2},$$

where n is the number of counterions per cubic centimeter in the bulk solution; δ is the thickness of the adsorbed monolayer; z is the valence; e the electronic charge; ϵ the dielectric constant for the solvent; ψ the electric potential at the interface; and κ^{-1} is the Debye–Hückel characteristic length. Π_{sr} is the short range repulsion term, and is expressed as

$$\Pi_{sr} = C_1\exp[-C_2(2h)],$$

where C_1 and C_2 are constants and are chosen such that the disjoining pressure curve has almost an infinite slope at a thickness $2h$ corresponding to the thickness 2δ ($(h_{ads} = \delta)$ of a Newton–Black film. A typical value for 2δ is 3 nm.

Figure B1 shows the plot of disjoining pressure as a function of thickness for a typical set of parameters used in obtaining the results of the "Results and Discussion" section.

Manuscript received Mar. 31, 1997, and revision received Aug. 1, 1997.